BOUNDARY-FITTED NONLINEAR-DISPERSIVE WAVE MODEL FOR APPLICATIONS IN GEOMETRICALLY COMPLICATED REGIONS

S. Beji[1], B.Barlas[2] and K. Nadaoka[3]

A nonlinear dispersive wave model in boundary-fitted coordinates is introduced for practical applications involving complicated lateral geometries. The model is formulated in terms of the contravariant velocity components so that the wall condition on irregular lateral boundaries is satisfied easily and accurately. Test cases involving converging, diverging, and circular channels are considered to check the reliability of the model predictions. Finally, nonlinear wave transformations in an arbitrarily shaped region are simulated as an example to practical applications.

Keywords: Boundary-fitted coordinates; nonlinear waves; non-rectangular physical domains.

1. Introduction

Practical applications in coastal engineering usually demand the solutions of the governing equations in geometrically complicated regions. Therefore, a circulation or a wave model expressed in boundary-fitted coordinates is much preferable. Earlier attempts were directed to transformation of the governing equations alone, keeping the cartesian velocity components unchanged as dependent variables. Later, it was recognized that transforming both the governing equations and the velocity components would be much better for accuracy and numerical stability (see Muin and Spaulding, 1996). In this work, one-component form of the nonlinear dispersive wave equations of Nadaoka *et al.* (1997) in boundary-fitted coordinates is introduced. The transformed equations are expressed in terms of the contravariant velocity components which render the specification of the lateral boundary conditions as simple as possible.

Several benchmark tests are considered for checking the reliability of the transformed equations and the numerical code. First, linear long wave propagation along a channel of gradually varying cross section is simulated to compare the amplitude variations against Green's analytical formula. Wave simulations in a circular channel are considered next to compare the numerically obtained solutions with the analytical solutions. The results for all the test cases indicate almost perfect agreement between the analytical and the numerical solutions. Finally, a hypothetical case of nonlinear wave propagation in an arbitrary domain is simulated as an example for practical applications.

[1]Professor, Department of Naval Architecture and Ocean Engineering, Istanbul Technical University, Maslak 80626, Istanbul, Turkey. sbeji@itu.edu.tr

[2]Assistant Professor, Department of Naval Architecture and Ocean Engineering, Istanbul Technical University, Maslak 80626, Istanbul, Turkey. barlas@itu.edu.tr

[3]Professor, Graduate School of Information Science and Engineering, Tokyo Institute of Technology, 2-12-1 O-okayama, Meguro-ku, Tokyo 152-8552, Japan. nadaoka@mei.titech.ac.jp

2. Wave Equations in Boundary-Fitted Coordinates

One-component form of the wave model of Nadaoka *et al.* (1997) in cartesian coordinates can be found in that particular work and are not repeated here. Using the well-known relations (see for example Hoffman and Chiang, 1995) and combining appropriate equations, the transformed forms of these equations in curvilinear coordinates (ξ, η, τ) become (Beji and Barlas, 2003)

$$\zeta_\tau + J\left[\left(C_p^2/g+\zeta\right)U^*\right]_\xi + J\left[\left(C_p^2/g+\zeta\right)V^*\right]_\eta = 0, \tag{1}$$

$$\begin{aligned} rJU_\tau^* &+ \xi_*^2 Q_\xi + \xi_*\eta_* Q_\eta \\ &= \frac{\xi_*^2}{\omega^2 C_p^2}\left[C_*\left(U_\xi^* + V_\eta^*\right)\right]_{\xi\tau} + \frac{\xi_*\eta_*}{\omega^2 C_p^2}\left[C_*\left(U_\xi^* + V_\eta^*\right)\right]_{\eta\tau}, \end{aligned} \tag{2}$$

$$\begin{aligned} rJV_\tau^* &+ \xi_*\eta_* Q_\xi + \eta_*^2 Q_\eta \\ &= \frac{\xi_*\eta_*}{\omega^2 C_p^2}\left[C_*\left(U_\xi^* + V_\eta^*\right)\right]_{\xi\tau} + \frac{\eta_*^2}{\omega^2 C_p^2}\left[C_*\left(U_\xi^* + V_\eta^*\right)\right]_{\eta\tau}, \end{aligned} \tag{3}$$

with

$$\begin{aligned} Q = g\zeta &+ \frac{1}{2}\left(1 - 3\omega^2 C_p^2/g^2\right)\left[\eta_*^2 U^{*2} + \xi_*^2 V^{*2} - 2\xi_*\eta_* U^* V^*\right] \\ \xi_*^2 &= \xi_x^2 + \xi_y^2, \qquad \eta_*^2 = \eta_x^2 + \eta_y^2, \\ \xi_*\eta_* &= \xi_x\eta_x + \xi_y\eta_y, \qquad C_* = C_p^4(1-r)J. \end{aligned} \tag{4}$$

where ζ is free surface elevation, $U^* = U/J$ and $V^* = V/J$ with U and V being the contravariant components of the horizontal velocity vector at $z = 0$. J is the Jacobian and $\xi_x, \xi_y, \eta_x, \eta_y$ are the metrics of the transformation. $r = C_g/C_p$ with C_p and C_g denoting respectively the phase and group velocities computed according to linear theory for a specified wave frequency ω and a given local depth h.

3. Numerical Approach and Boundary Conditions

Since the transformed computational domain is perfectly rectangular, the numerical solutions of equations (1-4) may be accomplished quite conveniently using finite-difference approximations. Figure 1 shows a sketch of an arbitrarily shaped physical domain and the corresponding computational domain.

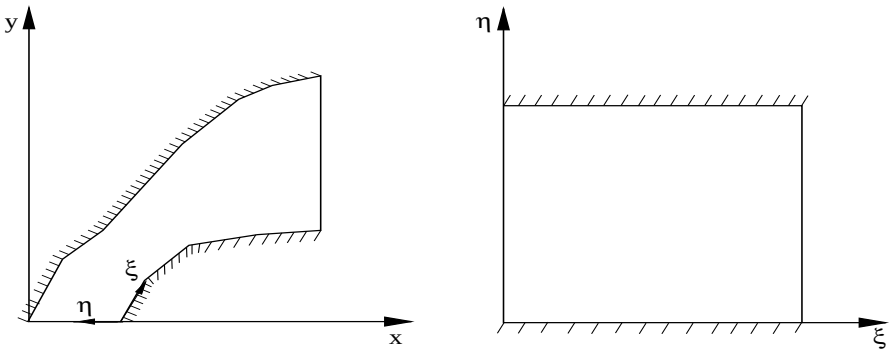

Figure 1. Definition sketch of the physical domain (left) and the corresponding computational domain (right). The hatched lines indicate wall boundaries.

After trying three different grid orientations (non-staggered grid, staggered Arakawa B-grid, and C-grid) it has been decided that staggered Arakawa C-grid performed best for the equations used here (Kantha and Clayson, 2000). Figure 2 shows the grid orientation for the variables.

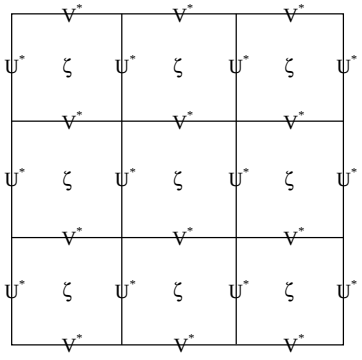

Figure 2. Grid orientation (staggered Arakawa C-grid) for the variables ζ, U^*, and V^*.

Two time levels are used and all the derivatives are centered at the mid-time level $t + \Delta t/2$, t being the current time and Δt the time step. The main wave propagation direction is taken along the positive $\xi-$axis; therefore, $\xi-$momentum equation is solved first to obtain U^* for the new time level $t + \Delta t$, assuming the new time level values of ζ and V^* known. Then, $\eta-$momentum equation is solved for V^* using U^* as computed from the previous step. Finally, the surface displacement is obtained from an explicit discretization of the continuity equation. Since all these computations involve certain approximations, an iterative procedure is adopted. Through numerical experiments it has been ascertained that for all the cases considered in this work, a maximum of five iterations were sufficient to obtain reliable results. This was determined by checking the values of the normalized surface elevation at selected locations between successive iterations until the difference between two consecutive iterations became less 10^{-4}.

Since the wave model is formulated in terms of the contravariant velocities, even for irregular geometries the wall condition can be specified in a quite straightforward manner by simply requiring the contravariant velocity component normal to the wall boundary vanish.

The radiation condition for outgoing waves usually requires particular attention due to undesirable reflection effects which contaminate the solution within the domain. The classical radiation condition for unidirectional waves is given by Sommerfeld's equation, which implies right or left going unidirectional waves of constant celerity. For the directional waves higher-order boundary conditions of Engquist and Majda (1977) may be used for better absorption of complicated wave patterns. However, even for directional waves, Sommerfeld's radiation condition in boundary-fitted coordinates is found to give quite acceptable results, while having relatively simpler expression. Sommerfeld's equations in curvilinear coordinates in the $\xi-$ and $\eta-$directions are

$$\begin{aligned}
\left(\xi_x\eta_y - \xi_y\eta_x\right) U^*_\tau \quad &\pm \quad C\left[\left(\xi_x^2\eta_y - \xi_y^2\eta_x\right) U^*_\xi + \eta_x\eta_y\left(\xi_x - \xi_y\right) U^*_\eta\right] \\
&\pm \quad C\xi_x\xi_y\left[\left(\xi_y - \xi_x\right) V^*_\xi + \left(\eta_y - \eta_x\right) V^*_\eta\right] = 0 \qquad (5) \\
\left(\xi_x\eta_y - \xi_y\eta_x\right) V^*_\tau \quad &\pm \quad C\left[\left(\xi_x\eta_y^2 - \xi_y\eta_x^2\right) V^*_\eta - \xi_x\xi_y\left(\eta_x - \eta_y\right) V^*_\xi\right] \\
&\pm \quad C\eta_x\eta_y\left[\left(\eta_x - \eta_y\right) U^*_\eta + \left(\xi_x - \xi_y\right) U^*_\xi\right] = 0 \qquad (6)
\end{aligned}$$

If the physical domain is rectangular, $\xi_x = 1$, $\xi_y = 0$, $\eta_x = 0$, and $\eta_y = 1$, the above equations reduce to $u_t \pm Cu_x = 0$ and $v_t \pm Cv_y = 0$, respectively. In this work the outgoing boundary is located at the end of the $\xi-$direction hence equation (5) with + sign (right going waves) is used.

4. Sample Computations

Computations involving non-rectangular lateral boundaries are presented now to demonstrate both the versatility of the equations derived and the accuracy of the numerical code. Wave simulations in gradually converging, diverging, and circular channels are performed for comparisons with the corresponding analytical results while a hypothetical case showing nonlinear wave propagation across a region enclosed by bending lateral walls is presented as an example to practical applications.

4.1 *Gradually Varying Channels*

Linear long wave propagation along a gradually converging channel is simulated first and the magnification of the wave amplitude is compared with the theoretical formula of Green. The period of the incident wave is $T = 8\ s$ and the water depth $h = 1\ m$, resulting in a wavelength of approximately $L = 25\ m$. The channel width reduces to half its initial value after a distance of 10 wavelengths. For a constant water depth Green's formula predicts an amplitude magnification according to

$$a(x) = a_0\sqrt{b_0/b(x)} \tag{7}$$

where x is the distance along the channel, a_0 is the initial wave amplitude and b_0 is the channel width at $x = 0$. $a(x)$ and $b(x)$ stand respectively for the amplitude and the channel width at an arbitrary location x along the channel (see Lamb, 1932, §185). Alternatively, equation (7) may be obtained from the principle of constancy of the energy flux across the channel. Figure 3a shows a perspective view of the fully-developed wave field while figure 3b compares the numerically computed wave form in mid-section with equation (7).

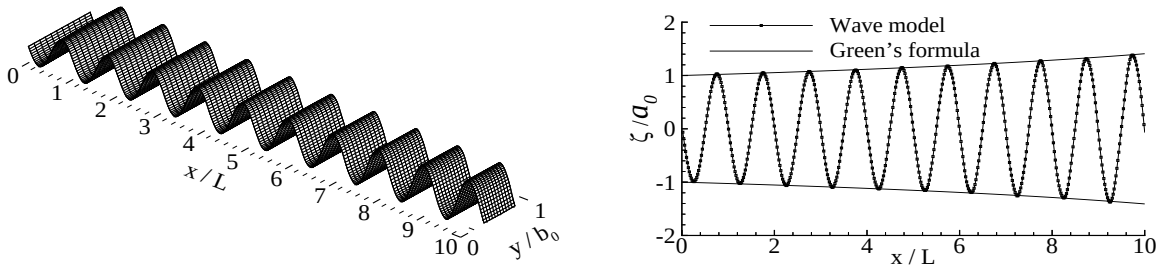

Figures 3a, b. Long wave propagation across a gradually converging channel: perspective view, and magnification of the simulated wave compared with the analytical expression.

The next case is a gradually diverging channel with incident wave and water depth conditions identical to the above case. The channel width doubles its initial value after 10 wavelengths and equation (7) is valid as given above. Figure 4a shows the perspective view and figure 4b compares the computed and theoretical values as in figures 3a, b.

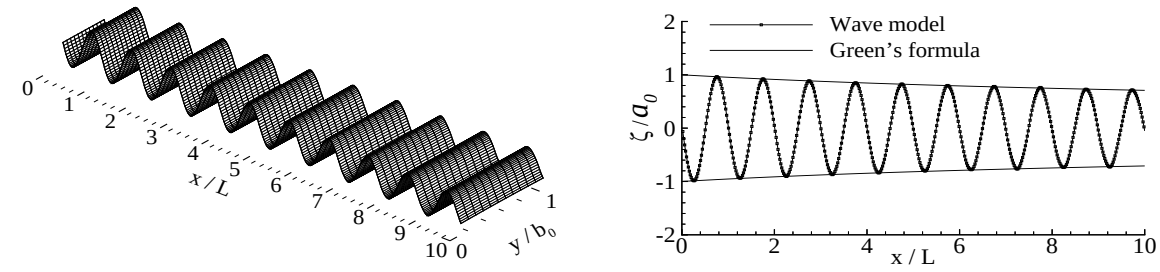

Figures 4a, b. Long wave propagation across a gradually diverging channel: perspective view, and attenuation of the simulated wave compared with the analytical expression.

From the figures 3b and 4b it is obvious that for both cases the numerically simulated amplitude magnification and attenuation agree almost perfectly with the corresponding analytical solutions.

4.2 *Circular Channel*

Equations (1-4) are now used for the simulation of waves in a circular channel. Since the analytical solution is available only for linear waves the simulations are performed for the linearized versions of the equations. In the context of acoustics, Rostafinski (1976) studied the sound propagation in a curved duct. The analytical solution, which may be readily adapted to the present problem, may be summarized as follows. In polar coordinates, $r = \sqrt{x^2 + y^2}$ and $\theta = \arctan y/x$, the surface elevation is expressed as a linear combination of different modes, which are given in terms of the Bessel functions of the first and second kind:

$$\zeta(r, \theta, t) = \sum_{n=1}^{N} \left[a_n J_{\nu_n}(kr) + b_n Y_{\nu_n}(kr)\right] e^{i\nu_n \theta} e^{i\omega t}, \tag{8}$$

where ν_n's $(n = 1, \cdots, N)$ are to be determined from equation (11) below. The boundary conditions on the inner wall and outer wall dictate $\partial\zeta/\partial r = 0$ so that

$$a_n J'_{\nu_n}(kr_i) + b_n Y'_{\nu_n}(kr_i) = 0, \tag{9}$$
$$a_n J'_{\nu_n}(kr_o) + b_n Y'_{\nu_n}(kr_o) = 0, \tag{10}$$

in which the primes denote differentiation with respect to r. Eliminating a_n and b_n from the above equations give the condition for determining ν_n's:

$$J'_{\nu_n}(kr_i)Y'_{\nu_n}(kr_o) - J'_{\nu_n}(kr_o)Y'_{\nu_n}(kr_i) = 0. \tag{11}$$

Imposing the incident wave amplitude as $\zeta(r, 0, t) = 1$ at the channel entrance $\theta = 0$, noting that each component function is orthogonal with weight $1/r$, the coefficients a_n and b_n are obtained as

$$a_n = Y'_{\nu_n}(kr_i) \frac{\int_{r_i}^{r_o} \frac{F_n(r)}{r} dr}{\int_{r_i}^{r_o} \frac{F_n^2(r)}{r} dr}, \qquad b_n = -\frac{J'_{\nu_n}(kr_i)}{Y'_{\nu_n}(kr_i)} a_n \tag{12}$$

where $F_n(r) = Y'_{\nu_n}(kr_i)J_{\nu_n}(kr) - J'_{\nu_n}(kr_i)Y_{\nu_n}(kr)$ is obtained from the use of (9) in (8). Also, note that a_n and b_n are related through the boundary condition (9).

For the test case considered here the inner radius of the channel is taken as $r_i = 100\ m$ and the outer radius as $r_o = 200\ m$; the channel covers an arc of 180^o. The water depth and the incident wave period are selected as $h = 10\ m$ and $T = 5\ s$, respectively. These parameters result in a wavelength of $L = 36.6\ m$ and wavenumber $k = 0.17\ rd/m$.

Using equation (8) the analytical solution is established from the superposition of $N = 6$ different modes which are determined as $\nu_n = 9.7, 16.0, 18.9, 22.1, 26.1, 31.8$ from equation (11) for $r_i = 100\ m$, $r_o = 200\ m$, and $k = 0.17\ rd/m$.

In numerical simulations, sinusoidal waves with a uniform amplitude are imposed across the channel at the entrance while equation (5) is used as the radiation condition at the end of the computational domain. In physical domain, a constant angular grid spacing of $\Delta\theta = \pi/360\ rd$ is used along the channel while the grid spacing in the radial direction is $\Delta r = 1\ m$. Time resolution is taken as $\Delta t = T/50$. No sponge layer was used at the outgoing boundary; however, the computational domain was 20% longer than shown to avoid the contaminating effects of reflected waves.

As the waves propagate in the circular channel, they reflect from the outer wall and diffract in the vicinity of the inner wall thus creating quite complicated patterns as depicted in the perspective views and contour plots given in figures 5a-d.

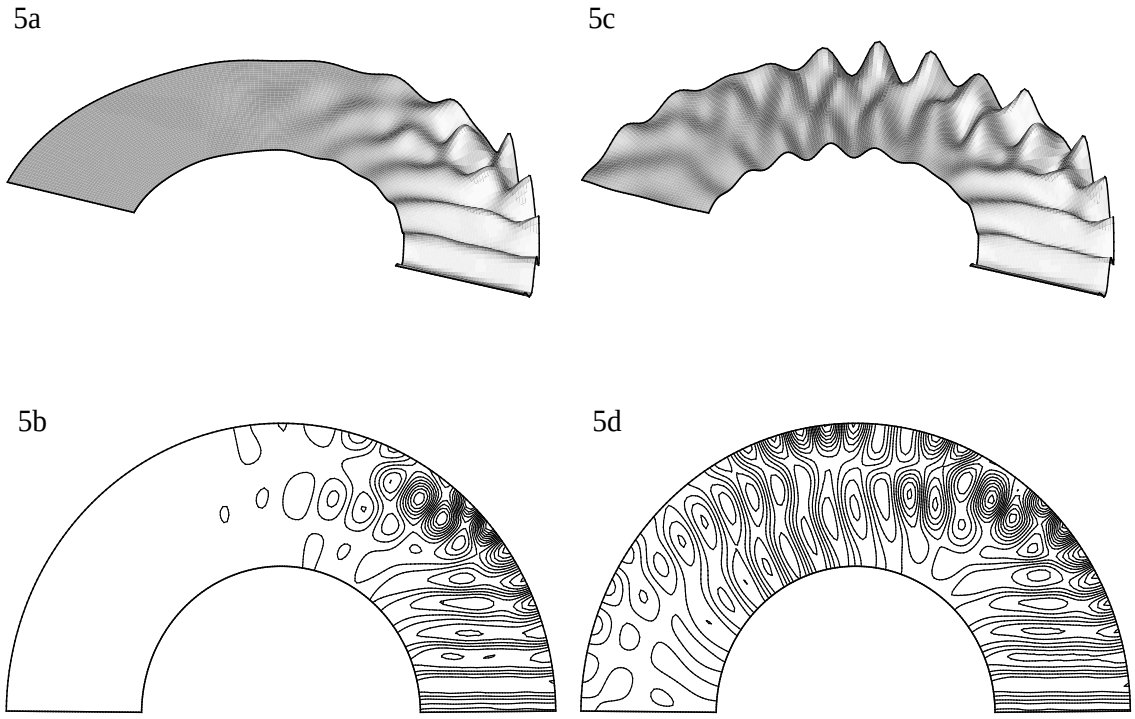

Figure 5a-d. Perspective views and contour plots of wave propagation in a circular channel at $t = 10T$ (left) and $t = 20T$ (right) as obtained from the numerical solution of the present model.

In order to make quantitative comparisons with the theory, the analytical solution is compared in figure 6 with the fully-developed wave field as obtained from the numerical solution after 40 wave periods elapsed. The two solutions appear identical, which establish confidence in the model equations and the numerical code.

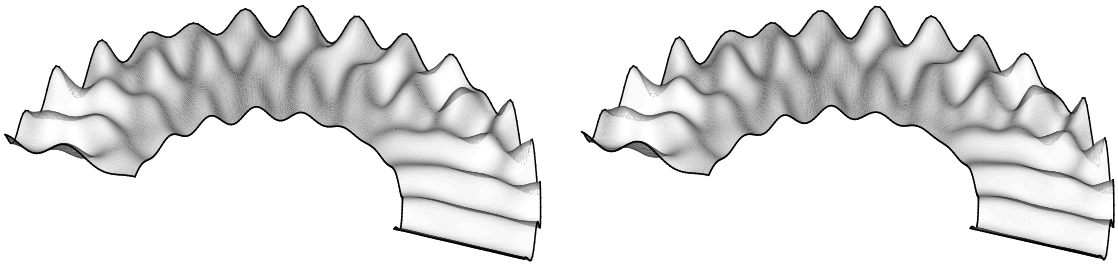

Figure 6. Fully-developed wave field in a circular channel: analytical solution (left) and numerical solution (right).

Finally, comparisons of the surface displacement along the inner wall and the outer wall between the analytical solution and numerical solution are presented in figures 7 and 8.

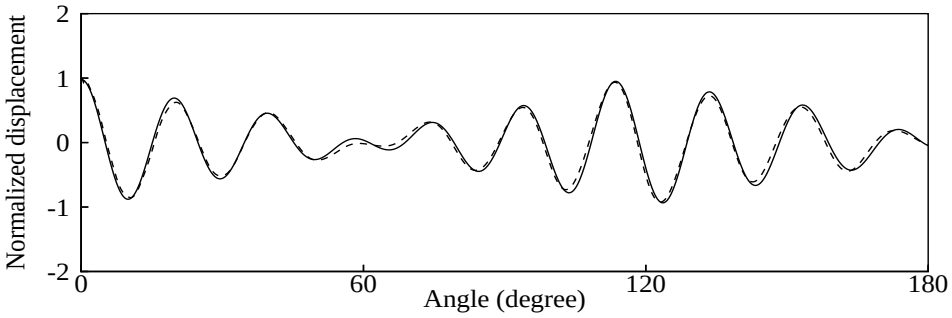

Figure 7. Comparison of the analytical solution (solid line) with the numerical solution (dashed line) for the surface displacement along the inner wall.

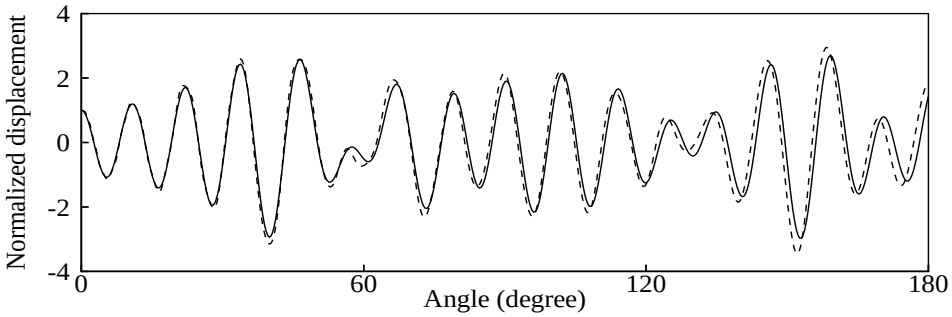

Figure 8. Comparison of the analytical solution (solid line) with the numerical solution (dashed line) for the surface displacement along the outer wall.

As the above figures reveal, except for slight phase differences, the agreement with the theory is excellent even for such a complicated case involving reflection and diffraction patterns. Thus, the test provides a definite conclusion regarding the reliability of the model introduced.

4.3 *A Hypothetical Case*

The last simulation is a hypothetical case showing nonlinear wave propagation across a region enclosed by bending lateral walls which cause diffraction (left wall, bending out) and reflection (right wall, bending in) of waves. The incident waves are Stokes type waves with period $T = 4\ s$, height $H = 0.7\ m$ and steepness $kH = 0.2$; the water depth is constant $h = 5\ m$. Figures 9a and 9b, depicted at two different instances, show that qualitative aspects of the wave deformations are well simulated and the nonlinearity of the wave field does not create any numerical problems.

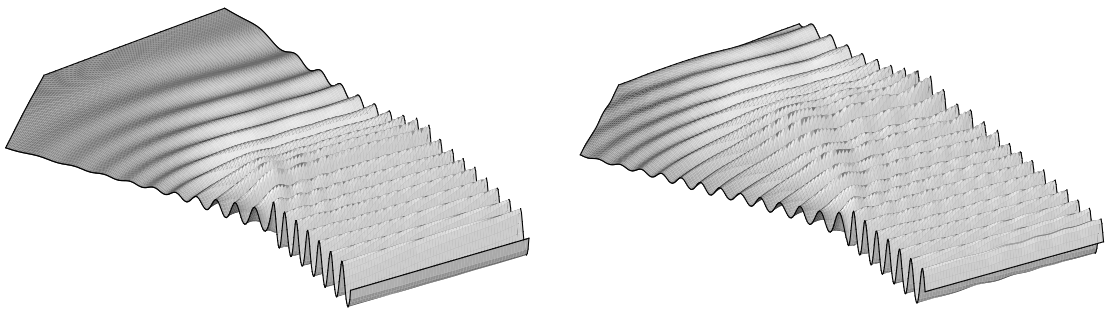

Figure 9a and 9b. Nonlinear wave propagation across a region of non-uniform cross section.

5. Concluding Remarks

A nonlinear dispersive wave model valid for arbitrary water depths is given in the boundary-fitted curvilinear coordinate system and the numerical code of these equations is developed. The comparisons for the test cases of gradually diverging, converging, and circular channels provide convincing evidence regarding the reliability and accuracy of the model equations and the numerical approach. A hypothetical case simulation involving nonlinear wave amplitudes and arbitrary lateral boundaries serves as an example to the possible practical applications of the model. Inclusion of the wave breaking effect, albeit in a semi-empirical manner, would be quite desirable especially in the simulations involving nearshore regions with man-made structures.

References

Beji S., Barlas B. (2003). Boundary-fitted nonlinear-dispersive wave model for regions of arbitrary geometry. Submitted to *Int. J. Num. Meth. in Fluids*

Engquist B,, Majda A. (1977). Absorbing boundary conditions for the numerical simulation of waves. Math. Comp.; **31**: 629-651.

Hoffmann K. A., Chiang S. T. (1995). *Computational Fluid Dynamics for Engineers.* Volume II, 3rd print. Wichita, Kansas: Engineering Education System; pp.451.

Kantha L. H. , Clayson C. A. (2000). *Numerical Models of Oceans and Oceanic Processes.* San Diego, California: Academic Press, pp.940.

Lamb, H. (1932). *Hydrodynamics*, New York, Dover Publications; pp.738.

Muin M., Spaulding M. (1996). Two-dimensional boundary-fitted circulation model in spherical coordinates. J. Hydr Eng; Sept.:512-21.

Nadaoka K., Beji S., and Nakagawa Y. (1997). A fully dispersive weakly nonlinear model for water waves. Proc R. Soc London A; **453**, 303-318.

Rostafinski, W. (1976). Acoustic systems containing curved duct sections. J. Acoust. Soc. Am.; **60**, 23-28.